Catal Lett (2015) 145:1446–1456
DOI 10.1007/s10562-015-1550-3

Catalytic Reduction of NO_X Over TiO_2–Graphene Oxide Supported with MnO_X at Low Temperature

Wei Su[1] · Xining Lu[1] · Shaohua Jia[2] · Juan Wang[1] · Hongzhi Ma[1] · Yi Xing[1]

Received: 26 March 2015 / Accepted: 6 May 2015 / Published online: 16 June 2015

Abstract TiO_2–graphene oxide (TiO_2–GO) nanocomposites were prepared by the sol–gel method with different mass ratios of GO. The MnO_X active components were loaded by means of ultrasonic impregnation. The catalysts exhibited excellent physical structures and electron transfer properties, which favored the catalytic activity. All of the catalysts were characterized by FESEM, XRD, TEM, BET, FT-IR, and XPS. The catalytic reduction activities of NO_X were studied under low temperature conditions using ammonia as the reductant. Results indicated GO formation in the TiO_2–GO supports, which reveals that TiO_2–GO can be readily indexed as anatase TiO_2 in all samples. Various valence states of manganese species coexisted in the MnO_X/TiO_2–GO catalysts. Non-stoichiometric (MnO_X/Mn) on the surface of the composite catalysts was particularly beneficial to electron transfer, resulting in good redox performance. The optimum mass ratio of Mn in MnO_X/TiO_2–0.8 % GO was 9 wt%, and catalyst with this amount of Mn exhibited good resistance to H_2O and SO_2. All of the samples showed excellent N_2 selectivity.

Graphical Abstract The surface of the GO sheets is covered by a uniform layer of MnO_X which increasing the activity of the catalyst by 9 % MnO_X/TiO_2–0.8 % GO.

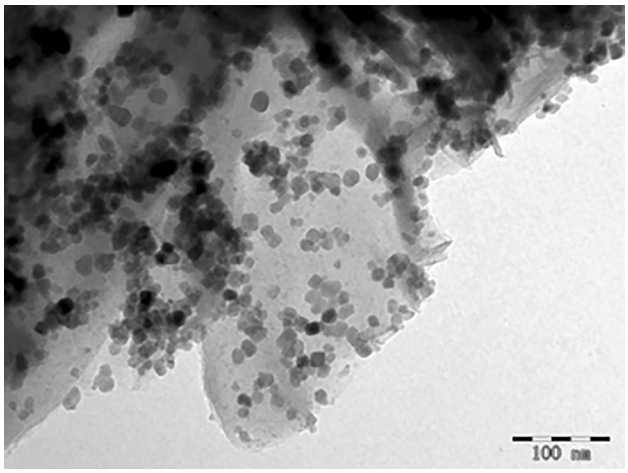

Keywords Graphene oxide · TiO_2–GO · Selective catalytic reduction · Low temperature · Manganese oxides

1 Introduction

NO_x (nitrogen oxides, mainly NO and NO_2) is one of the main pollutants in the atmosphere, however, over 95 % of the NOx in the atmosphere is NO. NO_2 is found in the air only in very small proportions. About 90 % of NO_x in the flue gas is NO, which mainly comes from vehicle exhaust, fossil fuel combustion, and emissions from stationary sources. NO can cause acid rain, photochemical smog, greenhouse effects, and damage to human health [1–3]. Selective catalytic reduction (SCR) methods aim to reduce NO_x in flue gas to N_2 using a reducing agent such as NH_3; this reaction must be controlled at a certain temperature with a certain amount of oxygen content, and using specific

✉ Hongzhi Ma
mhz527@sina.com

Wei Su
suwei@ustb.edu.cn

[1] Key Laboratory of Educational Ministry for High Efficient Mining and Safety in Metal Mine, University of Science and Technology Beijing, 30 Xueyuang Road, Haidian District, Beijing 100083, China

[2] School of Environment, Tsinghua University, Beijing, China

catalysts. The most mature commercial catalyst for this process is V_2O_5–WO_3/TiO_2, however, the temperature window of the catalyst is between 350 and 400 °C. Thus, SCR devices must be placed before the air pre-heater, particularly because poor N_2 selectivity and high SO_3 conversion rates are evident at this temperature range [4]. If the SCR reactor is placed after the electrostatic precipitator and desulfurization devices, the effects of SO_2 and dust alkaline earth metal on the SCR catalysts can be reduced significantly. The outlet temperature of flue gas during sintering after semi-desulfurization is generally about 80–150 °C. If flue gas reheating cannot be introduced, the cost of de-nitration can be significantly reduced [5]. Hence, developing efficient and economic catalysts at lower temperatures, specifically at 80–180 °C, is a popular focus of research on de-nitrification of sintering flue gas. Research on the effects of complex cryogenic stage as sintering flue gas to low temperature catalyst is still at the blank stage.

Researchers have carried out many in-depth studies on SCR catalyst supports at low temperature as well as their active components. Findings indicate that Mn-based catalysts exhibit good low temperature catalytic properties [6, 7]. In addition, anatase TiO_2 is often used as a support of SCR catalysts because of its good mechanical and strong resistance to sulfuration properties [8]. However, the small specific surface area and poor thermal stability of the material have restricted its catalytic properties to some extent [9, 10]. Carbon-based materials (e.g., activated carbon, carbon fibers, carbon nanotubes, etc.) have larger specific surface areas and better chemical stability; thus, these materials have been used as a supports in SCR $DeNO_x$ experiments [11–14]. Mn-based catalysts with carbon-based materials as supports, such as MnO_X/ACF [11], MnO_X/AC/ceramic, [12] and MnO_X/MWCNTs (manganese oxides supported on multi-walled carbon nanotubes), have been widely used in research and can yield good SCR performance at temperatures below 250 °C. Zhao Xueying and other researchers [15] have prepared TiO_2–CNT composite powder materials of different mass ratios by the sol–gel method. Results show that this method allows anatase nano-TiO_2 to be evenly distributed on the CNT surface so that agglomeration of TiO_2 solution molecules is effectively inhibited during hydrolysis. Graphene oxide (GO) and graphene (GE) are new nanoscale carbon materials bearing the basic features of not only carbon-based materials but also surface active groups with electron transfer ability, especially during GO preparation to promote oxidation. SO_4^{2-} is formed on the catalyst surface by addition of a large quantity of concentrated sulfuric acid, which plays a role of pre-sulfuration to the support and this feature will necessarily improve the resistance to poisoning of catalyst to SO_2. Currently, composite supports of TiO_2–GO and TiO_2GE are only used in photo catalysis, although their characteristics may also be applicable in denitration by SCR at low temperatures. Yang et al. [16] found that –OH, –COOH, and other oxygen-containing functional groups can improve CNT dispersion in water and enhance particle interactions with the substrate to improve the catalytic activity of the SCR reaction. GO surfaces also have these functional groups.

In this paper, pertinent to the outlet temperature of desulfurization process by semi-dry flue gas sintering, the temperature range of 80–180 °C is selected. MnO_X/TiO_2–GO catalysts were prepared using the sol–gel method and ultrasonic impregnation. The TiO_2 in the TiO_2–GO supports were anatase in structure, which is conducive to enhancing SCR catalytic activity. XRD characterization confirms that introduction of GO does not affect polymorphs of TiO_2. Using field emission scanning electron microscopy (FESEM), EDS spectrum analysis, X-ray diffraction (XRD), Brunauer–Emmett–Teller analysis (BET), transmission electron microscopy (TEM), X-ray photoelectron spectroscopy (XPS), and Fourier transform infrared (FT-IR) spectroscopy, interactions among the GO support, TiO_2, and MnO_X were further explored to determine why SCR reactivity is improved under specific conditions. The effects of H_2O and SO_2 on the catalysts and the resistance to poisoning mechanism were investigated to provide theoretical guidance for future research on low temperature SCR catalysts for sintering flue gas and their industrial applications.

2 Materials and Methods

2.1 Catalyst Preparation

2.1.1 Preparation of TiO_2–GO Supports

In the experiments, an improved Hummers method was applied to prepare GO [17, 18]. Firstly, 23 ml of concentrated H_2SO_4 was placed in a 1000 ml beaker. Graphite flakes weighing 1 g and $NaNO_3$ weighing 0.5 g (Kim Electronic Materials Plant, Lacey City of Qingdao Municipality) were slowly added to concentrated H_2SO_4 at moderate stirring speed and in an ice bath to maintain the temperature and prevent the bump splash of reaction. When the chemicals had been sufficiently dissolved and uniformly mixed, 3 g of $KMnO_4$ was slowly added to the mixture at vigorous stirring speed. A thermometer was used to monitor and maintain the temperature below 20 °C.

Upon addition of $KMnO_4$, a violent reaction took place and the color of the liquid in the beaker changed from black to dark green. Upon complete dissolution of $KMnO_4$, the ice bath was removed and a water bath at a temperature of 35 ± 3 °C was used instead. The liquid remained

incubated for 30 min. The contents of the beaker began foaming and turned into a black paste-like substance. Following this development, 46 ml of de-ionized water was added to the solution under stirring. The paste-like material became thinner and was accompanied by strong bubbling. The beaker was moved to a water bath at 90 °C. Incubation was performed for another 15 min, and the beaker was transferred to an ice bath. The liquid in the beaker was diluted to 140 ml using warm de-ionized water and stirred continuously for 5 min. Finally, H_2O_2 was gradually added to the solution until a color change to bright yellow, which signifies completion of oxidation.

The resulting solid filter cake was obtained after suction filtration. About 500 ml of 10 % hydrochloric acid was used to clean the cake, followed by three cycles of final washing. Solid oxidized graphite was obtained. To remove impurities from strong oxidants introduced to the reaction, the resulting solid material was centrifuged for 30 min at a speed of 4000 r min^{-1} for three cycles. Finally, the solid material was dried in an 80 °C air-blowing drying chamber for 12 h to obtain flaky black solid GO. After dissolving in deionized water and sonicating for 2 h, the layers of the GO flakes were stripped to prepare the GO solution. A certain volume of tetra-*n*-butyl titanate and ethanol were vigorously stirred to obtain solution A. Glacial acetic acid, the GO solution (different concentrations based on mass ratio; 30 min of ultrasound was applied to release the flake structure of GO prior to use), and anhydrous ethanol were dissolved to obtain solution B. Solution B was slowly dropped into solution A, and 90 min of continuous stirring was performed to obtain a yellow–brown homogeneous titanium–GO solution. Brown crystals were obtained after aging of this sol at room temperature for 24 h and then drying at a constant temperature of 80 °C for 12 h to remove the organic solution. Finally, the support was ground, calcined in a tubular furnace in a nitrogen atmosphere, and kept warm at 450 °C for 6 h to obtain the TiO_2–GO power. In experiments based on aqueous solutions of various concentrations, TiO_2–GO supports with different mass percentages were prepared as follows: TiO_2–2 % GO, TiO_2–0.8 % GO, TiO_2–0.4 % GO, and TiO_2–0.2 % GO.

2.1.2 *Preparation of MnO_X/TiO_2–GO Catalysts by Ultrasonic Impregnation*

Using manganese acetate ($C_4H_6MnO_4{\cdot}4H_2O$) as a precursor linked to the active component on the support, both liquor and support were mixed and treated by an ultrasonic device at 60 °C for 90 min to ensure full contact with the support and that the active components are uniformly attached to the surface of the support. The catalysts were placed in an oven set to 80 °C for drying. The materials were burned at 450 °C for activation in a nitrogen atmosphere and incubated for 3 h to prepare supported catalysts MnO_X/TiO_2–GO: X % MnO_X/TiO_2–GO where X % stands for the mass percentage of Mn elements in MnO_X/TiO_2–GO.

2.2 Catalyst Characterization

Microscopic characterization of the morphology of catalyst was performed using a Hitachi S4800 field emission scanning electronic microscope.

An X Flash Detector Type 5010 (BRUKER) to analyze elemental distributions on the surface of the catalysts.

Phase analysis of sample materials was done using a Rigaku DMAX-RB 12 kW rotating anode X-ray diffractometer. A copper target (wavelength, 0.15406 nm), 40 kV acceleration voltage, 150 mA current intensity, 10° min^{-1} scanning speed, and scanning range $2\theta = 10°$–$100°$ were applied.

A QuadraSorb SI type analyzer was applied to determine the specific surface areas and pore structure parameters of the catalyst via the static nitrogen physical adsorption method.

By means of NEXUS 670 type FT-IR infrared instrument made by Thermo Nicolet samples were tested for Fourier transformation infrared spectroscopy. Samples were prepared by use of potassium bromide KBr Tablet. Before the test N_2 was applied to blow off the impurities produced during the reaction process followed by sampling and analysis. The wave number used for the test was 400–4000 cm^{-1}.

A Kratos Axis Ultra DLD multifunctional electronic spectrometer was used to analyze the XPS spectra of the catalysts. This instrument was coupled to a monochromatic Al Kα anode target and multi-channel delay detector. The whole spectrum scanning of 160 eV and narrow spectrum scanning of 40 eV. The analytical results were calibrated using the C 1s binding energy.

A JEOL JEM-2100HR high resolution transmission electronic microscope was used to observe the microstructural features of grouped samples loaded with active components.

2.3 Catalyst Activity Testing

Steady-state SCR reaction experiments were performed in a quartz tube fixed-bed continuous flow reactor using 500 mg catalyst of 60–100 mesh. The inner diameter of the quartz reaction tube was 9 mm, the reactor was placed in an electrically heated furnace with a programmable controller. The typical reactant gas composition included 0.1 vol% NO, 0.1 vol% NH_3, 7 vol% O_2, 10 vol% H_2O (when used), 200 ppm SO_2 (when used) with a balance of Ar. The Ar flow gas was divided into two branches. One branch converged with NO, NH_3, O_2, and SO_2 to form the main gas flow, while the other one passed through a heated gas-wash bottle containing

deionized water to introduce water vapor into the system when required. The feed flow rate was fixed at 600 ml min^{-1}, which were controlled by mass flow controllers and corresponded to a gas hourly space velocity (GHSV) of 67,000 h^{-1}, and the reaction temperature ranged from 80 to 180 °C. To test water resistance, H_2O was added using a controlled evaporator mixer. In resistance to poisoning experiments, the SO_2 concentration was 200 ppm. In selectivity tests, the content of N_2 in the vent served as a reference. A gas chromatograph (GC 7890A; Agilent Company; United States) was applied with Ar as the support gas.

Using a Thermo Scientific 42i-HL flue gas analyzer, the concentration of NO_x at the inlet and the outlet was determined to calculate the removal rate of NO_x. Taking into account the effect of gas adsorption on the catalyst, NO was fed into the reactor at the initial stage of the experiment. When the concentration at the outlet had stabilized, NO_X was fed into the reactor until the concentration of NH_3 at the outlet was stable upon reading the data. The removal rate of NO_x and selectivity of N_2 were obtained using Formulas (1) and (2), respectively. Here, $C^{in}_{NO_x}$, $C^{in}_{NO_2}$, and $C^{in}_{NH_3}$ respectively represent the concentrations of NO_X, NO, and NH_3 at the inlet. In the experimental system, only NO gas was fed into the reactor. However, because NO inevitably reacts with O_2 in the air and generates NO_2, we indicate the final results as NO_X. $C^{out}_{NO_x}$ and $C^{out}_{NO_2}$ represent the concentrations of NO_X and NO_2, respectively, and $C^{out}_{N_2O}$ represents the concentration of N_2O at the outlet.

$$NO_X \text{ conversion } (\%) = 100 \times \frac{C^{in}_{NO_X} - C^{out}_{NO_X}}{C^{in}_{NO_X}} \quad (1)$$

$$N_2 \text{ selectivity } (\%) = 100 \times \frac{C^{in}_{NO} + C^{in}_{NH_3} - C^{out}_{NO_2} - 2\,C_{N_2O}}{C^{in}_{NO} + C^{in}_{NH_3}} \quad (2)$$

3 Results and Discussion

3.1 SCR Activity of MnO_X/TiO_2–GO Catalyst

3.1.1 Effect of Different Mass Ratios of GO

Figure 1 shows the NH_3-SCR activity of 5 % Mn/TiO_2–GO catalysts with different mass ratios of GO.

Comparing with sample of only Mn/TiO_2 or Mn/GO support, the rising trend of the curve in Fig. 1 shows that increasing the amount of GO in the support increases the SCR activity of the catalyst and reached the maximum when Mn/TiO_2 mixed with 0.8 % GO, activity up to 93.38 % at 180 °C, especially, the catalytic activity of 5 % Mn/TiO_2–0.8 % GO was obviously better than the other

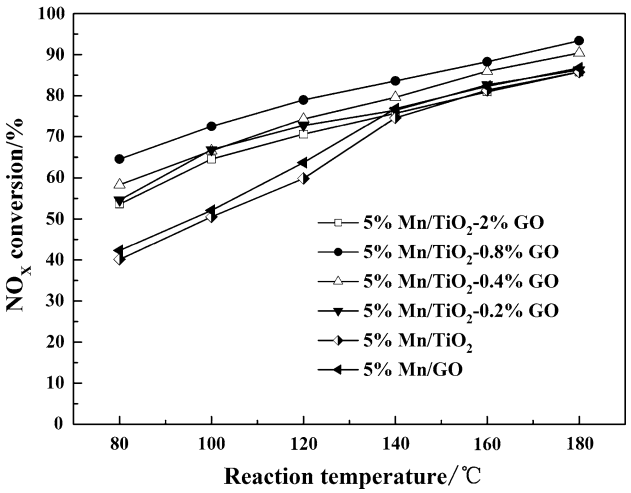

Fig. 1 Effect of different mass ratios of GO of Mn/TiO_2–GO catalysts on catalytic activity

samples at the low temperature range of 80–120 °C. When the amount of doped GO reached 2 %, the catalyst activity of 5 % Mn/TiO_2–2 % GO began to decrease, possibly because of clogging of the pore structures. This observation shall be discussed further in terms of BET analysis of the supports. As the GO content increased, the activity of the 5 % Mn/TiO_2–GO catalyst significantly improved compared with those of the 5 % Mn/TiO_2 and 5 % Mn/GO single-component catalysts in the low temperature range of 80–180 °C. As the reaction temperature increased, the curves of the activity of all samples converged. Taken together, results indicate that TiO_2–0.8 % GO is the best catalyst support for this experiment; as such, this catalyst was used for subsequent experiments and research.

3.1.2 Effect of Different Mn Loading and N_2 Selectivity

Figure 2a, b indicate the relationships between different Mn loadings in the Mn/TiO_2–0.8 % GO catalysts respectively, and the removal rate of NO_X and N_2 selectivity. Mn loadings of 0, 3, 5, 7, 9, and 11 % were applied in this experiment.

Figure 2a shows that increasing the Mn loading increases initially and then decreases the SCR activity of the Mn/TiO_2–0.8 % GO catalysts. When the Mn loading of the catalysts reached to 9 %, the maximum removal rate of NO_X up to 95 % at 180 °C. As the Mn loading increased to 11 %, the activity began to decline due to agglomeration of excess MnO_X particles on the surface of the TiO_2–0.8 % GO support. Nevertheless, the results were further elaborated by the following TEM and BET analysis.

Figure 2b shows the N_2 product selectivity and N_2O formation for these catalysts. All of the samples show high N_2 selectivity over the entire reaction temperature range

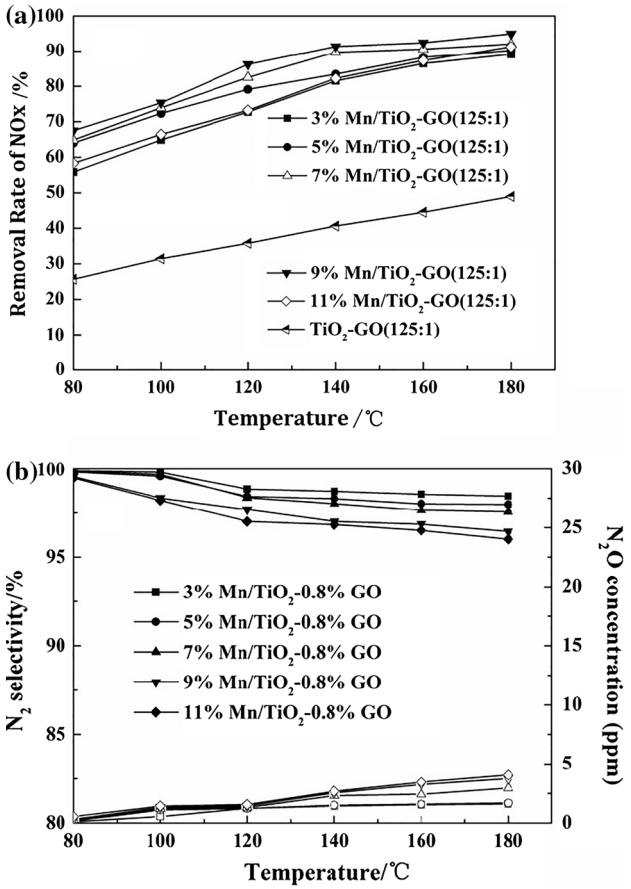

Fig. 2 **a** Effect of different Mn loadings on the removal rate of NO_X. **b** N_2 selectivity and N_2O formation over the various MnO_X/TiO_2–GO catalysts. Reaction conditions 0.1 vol% NO, 0.1 vol% NH_3, 7 vol% O_2, Ar to balance, GHSV 67,000 h^{-1}, 500 mg of catalysts

(all greater than 96 %). With increasing loading of the active component and reaction temperature, N_2 selectivity in the catalysts showed a downward trend, although N_2O levels generated remain low (<5 ppm). This result is due to N_2O generation and NH_3 oxidation reactions occurring at higher temperatures. Singoredjo [19] and other researchers found that, in MnO_X/Al_2O_3 catalysts, increases in Mn loading and reaction temperature generates greater amounts of N_2O and reductions in N_2 selectivity. These results resemble findings in this experiment.

3.2 Catalyst Characterization Results

3.2.1 FESEM Morphology of the Support and Scanning Analysis of the EDS Surface

Figure 3 shows the FESEM patterns of GO and the TiO_2–0.8 % GO support as well as scanning analysis results of the EDS mapping of the TiO_2–0.8 % GO support; these results are used to observe the morphology of the support and the distribution of each element in the support surface.

The monolayer morphology of the prepared GO is shown in Fig. 3a. Figure 3b, c show the lamellar morphology and the cross-sectional topography of the TiO_2–0.8 % GO support. The figures show that tiny white TiO_2 particles are uniformly distributed on the surface layer of flaky GO. In the cross-sectional diagram, several stacked GO layers can be observed. Further, EDS mapping analysis proved that the TiO_2 particles in TiO_2–0.8 % GO were distributed on the surface of GO. Figure 3d–f represent the respective distribution statuses of C, O, and Ti on the surface of the support. The three elements were integrated in an orderly and tight manner, which confirms that the TiO_2–GO supports prepared in this experiment present a uniform composition, which helps increase the specific surface area of the support, improves the pore structure characteristics of the support, and promotes uniform loading of the active component.

3.2.2 XRD Analysis Results of the Support

Figures 4a–c show the XRD spectra of as-received flaky graphite, GO, and TiO_2–GO supports with different mass ratios respectively.

Figure 4a demonstrates that the flaky graphite sample acquired for this experiment has high purity, and the graphite peaks appear only at around $2\theta = 26°$. No impurity peaks were observed for this material. Characteristic GO peaks appeared at a 2θ value of 9° in Fig. 4b. This small angular offset of the characteristic peaks shows excellent oxidation of GO in the present experiment. The absence of characteristic peaks at $2\theta = 26°$ indicates that the flaky graphite was completely oxidized to GO. The XRD spectra of TiO_2–GO with different mass ratios in Fig. 4c illustrates that all of the samples have characteristic GO peaks present at $2\theta = 9°$, which confirms successful combination of GO and TiO_2. Anatase TiO_2 had rich active sites, which enhanced the SCR activity of the catalyst, and the peaks at 2θ value of 25.3°, 37.8°, 48.1°, 53.9°, 55.0°, 62.7°, 68.7°, 70.3° and 75.1° were indexed to (101), (004), (200), (105), (211), (204), (116), (220) and (215) crystal planes (JCPDS 21-1272). Here, increases in mass ratio of TiO_2–GO, slightly decreases and broadens the intensity of diffraction peaks. These findings indicate that introduction of GO does not alter the crystal structure of TiO_2 and that the support completely maintains its anatase structure. This outcome is consistent with the research of previous scholars [20, 21].

3.2.3 TEM Analysis of MnO_X/TiO_2–GO Catalyst

Figure 5 shows TEM images of the Mn/TiO_2–0.8 % GO catalyst with different Mn loadings. The distribution of the active component particles were dispersed well on the lamellar GO.

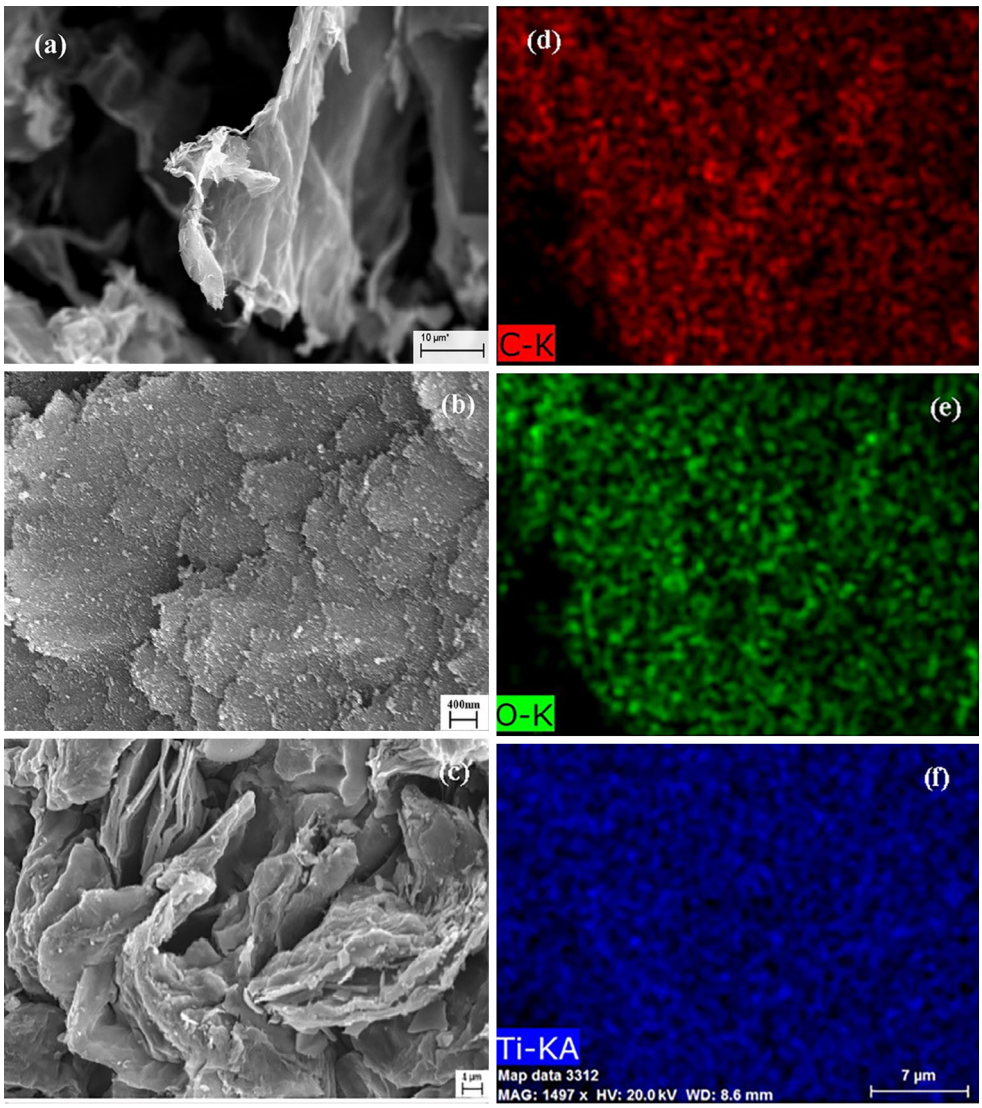

Fig. 3 FESEM patterns of the support and EDS energy pattern **a** GO, **b**, **c** TiO_2–0.8 % GO, and **d**, **f** EDS mappings of the TiO_2–0.8 % GO support

As shown in Fig. 5a–c, only a small amount of MnO_X particles are supported on the support surface. As the Mn loading continues to increase up to 9 wt%, the surface of the GO sheets is covered by a uniform layer of MnO_X particles with sizes ranging from 10 to 40 nm. They are all mesoporous materials. However, manganese particles appeared severe agglomeration when the manganese loading was increased to 11 wt%. Mutual coverage by MnO_X particles masks some of the active sites and reduces opportunities for contact with NH_3, thereby decreasing the activity of the catalyst. These characterization results verify our previous inference on changes in catalyst activity with varying Mn loadings.

3.2.4 BET Surface Areas and Pore Size Distributions

The detailed textural data of the specific surface area and pore structure of catalysts are shown in Table 1.

Analysis of the results of pore structure in Table 1 indicated that the specific surface area and pore volume of TiO_2–GO increase first by added GO, and average pore size showed the opposite trend, reaching a maximum when the mass ratios of GO reached 0.8 %. The distribution of pore sizes in all of the samples fell within 2–10 nm, which indicated that all of the samples are mesoporous materials.

However, when the mass ratios of GO reached 2 %, the specific surface area appeared to decrease. This was due to the excess GO caused agglomeration which had blocked some mesopores and micropores, resulting in the slight decline in the specific surface area. This result also verifies the cause of the change in catalytic activity with respect to mass ratio. Analysis of the results in the given table shows that as the MnO_x loading increases, the specific surface area and pore volume of Mn/TiO_2–GO catalyst slightly decrease before reaching the catalytic activity expected at optimal loading. Beyond a certain loading, however,

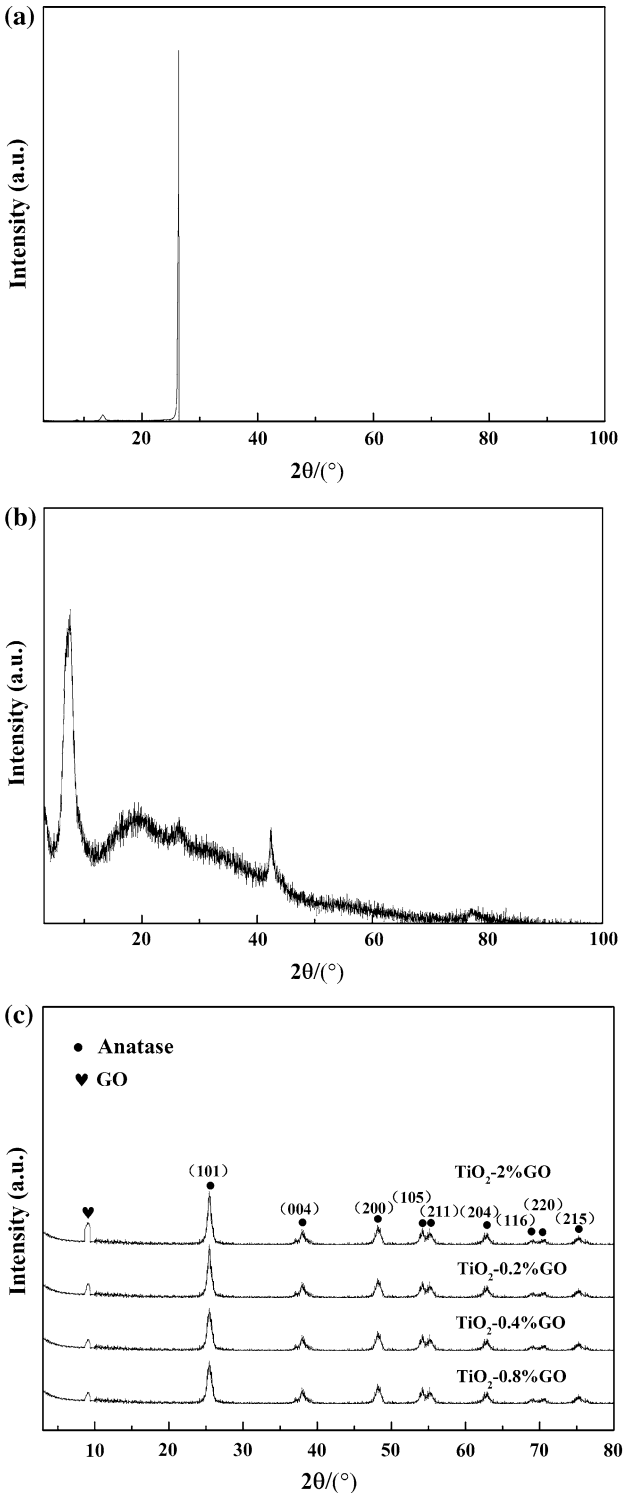

Fig. 4 XRD spectra of **a** as-received graphite, **b** GO, and **c** TiO_2–GO of different mass ratios

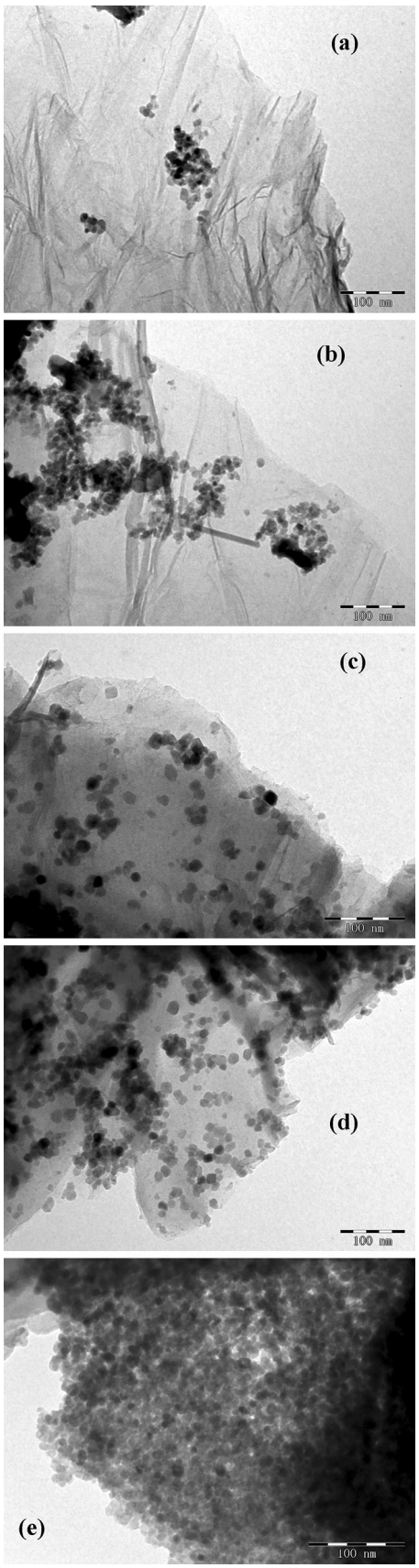

Fig. 5 TEM images of different Mn loading catalysts **a** 3 % MnO_X/TiO_2–0.8 % GO, **b** 5 % MnO_X/TiO_2–0.8 % GO, **c** 7 % MnO_X/TiO_2–0.8 % GO, **d** 9 % MnO_X/TiO_2–0.8 % GO, and **e** 11 % MnO_X/TiO_2–0.8 % GO

significant decreases in activity were observed. This tendency agrees with the trend previously reported by scholars. The specific surface area and pore volume of carbon-based supports, such as AC [22], ACF [23], and MWCNTs [24], decline after loading with metal oxides. In this experiment, the same trend was observed in the TiO_2–GO support after MnO_X loading. Upon analysis, incorporation of GO appeared to provide TiO_2 with the characteristics of carbon-based materials. When the MnO_X loading exceeded a critical value, as shown by the TEM morphology in the previous section, agglomerated was an important reason for the significantly reduced of the catalyst activity. Therefore, the catalytic activity of carbon-based titanium in this experiment is dependent not only on the specific surface area but also pore structure of the catalyst. Further analysis of the effect of additional GO on the redox capacity of catalyst must be performed through XPS.

3.2.5 XPS Analysis of the MnO_X/TiO_2–GO Catalysts

The concentrations of elements of MnO_X/TiO_2–0.8 % GO on the catalyst surface in Table 2. Figure 6 shows XPS analysis results of the 9 % Mn/TiO_2–0.8 % GO catalyst; Fig. 6a shows XPS spectrum of C 1s, while Fig. 6b–d illustrate the XPS spectra of Ti 2p, Mn 2p, and O 1s, respectively.

The surface element concentrations of the 9 % Mn/TiO_2–0.8 % GO catalyst as well as its valence states were further analyzed by XPS with reference to the NIST XPS database to compare peaks obtained under different energy bindings. Figure 6a shows two main peaks at 285.0 and 286.6 eV, respectively, representing amorphous carbon and graphite carbon from GO, may also be observed [25, 26]. The weak peak appearing at 289.2 eV is attributed to O=C–O [27]. Oxygen-containing groups present in GO provide an abundance of active sites for connecting GO to TiO_2 particles. This result suggests that, –OH on the surface of TiO_2 particle may reacts with –COOH and C–OH functional group, the surface is formed GO O=C–O–Ti, and C–O–Ti bond respectively by esterification and dehydration reactions, to achieve a closer integration [28]. XPS analysis detected the atomic surface compositions of fresh 9 % Mn/TiO_2–0.8 % GO catalysts.

From the XPS Ti 2p spectrum in Fig. 6b, two distinct curves which are Ti 2p1/2 and the Ti 2p3/2 spin–orbit splitting peaks at the binding energy of 464.3 and 458.6 eV are assigned to Ti^{4+}. De-convolution peaks of the Ti 2p spectrum also appeared at binding energies of 465.8 eV (Ti 2p1/2) and 460.2 eV (Ti 2p3/2). By referring to the XPS database, the peaks were identified as two characteristic spectra line of Ti–C. The results show a combination of chemical bonds between TiO_2 and GO. The characteristic XPS spectra line of Mn 2p and O 1s can be seen in Figs. 6c, d,

Table 1 Structural parameters of TiO_2, TiO_2–GO, and MnO_X/TiO_2–GO

Catalyst	Specific surface area ($m^2\ g^{-1}$)	Pore volume ($\times 10^{-2}\ cm^3\ g^{-1}$)	Average pore size (nm)
TiO_2	49	8.17	6.1
TiO_2–2 % GO	150	28.21	9.0
TiO_2–0.8 % GO	160	32.65	8.4
TiO_2–0.4 % GO	153	30.43	9.0
TiO_2–0.2 % GO	149	27.87	9.3
3 % Mn/TiO_2–0.8 % GO	158	32.43	8.4
5 % Mn/TiO_2–0.8 % GO	154	32.32	8.6
7 % Mn/TiO_2–0.8 % GO	152	32.10	8.7
9 % Mn/TiO_2–0.8 % GO	149	30.48	9.0
11 % Mn/TiO_2–TiO_2–0.8 % GO	137	27.87	9.2

Table 2 Atomic surface compositions of 9 % Mn/TiO_2 and 9 % Mn/TiO_2–0.8 % GO on the surface of the catalyst

Catalyst	Atomic composition(%)									
	C	Mn	Ti	O	O		Mn			
					O_α	O_β	MnO	MnO_2	Mn_2O_3	MnO_X/Mn
9 % Mn/TiO_2–0.8 % GO (fresh)	18.32	7.21	18.71	55.91	15.67	40.24	1.63	3.33	1.03	1.22
9 % Mn/TiO_2	–	6.41	42.56	51.03	12.87	38.16	–	3.28	3.13	–

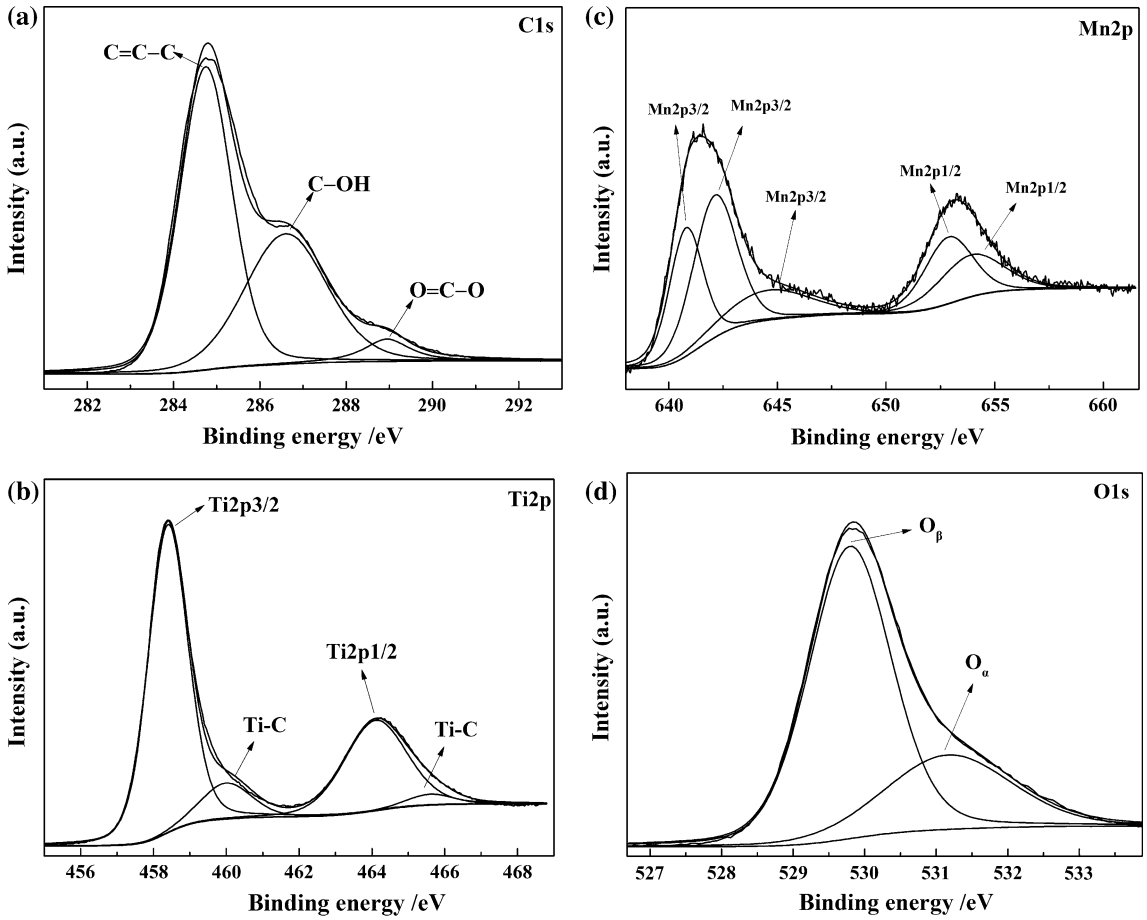

Fig. 6 XPS spectrum of 9 % Mn/TiO_2–0.8 % GO catalyst

wherein Mn exists in multiple forms, such as MnO, MnO_2, Mn_2O_3, and MnO_X/Mn, in the catalyst. Fitting of the deconvolution peaks showed three peaks of Mn 2p3/2 at binding energies of 640.8 eV (MnO), 642.0 eV (Mn_2O_3), and 643.4 eV (MnO_2). Two peaks, 652.9 eV (MnO_X/Mn) and 653.4 eV (MnO), belong to Mn 2p1/2. Results showed that the MnO and MnO_X/Mn contents of the fresh 9 % Mn/TiO_2–0.8 % GO catalyst obviously increased relative to those in the catalyst without GO, the results were consistent with the research achievements of Lu [29] before. The variety of MnO_X species with different valences present in the catalyst, especially non-stoichiometric MnO_X/Mn, activated electron mobility in the catalyst, which favors the redox reaction of the catalyst and further increases the removal rate of NO_X in SCR reaction [28]. In Fig. 6d, XPS fitting of separated peaks of O 1s demonstrates two types of O in the catalyst: lattice oxygen on the surface of the catalyst (529.4–530.1 eV, denoted as O_β) and chemisorbed oxygen (531.3–532.3 eV, denoted as O_α). Here, chemical adsorption of oxygen as O_2^{2-} or O^- occurs in the form of OH^- and carbonate (CO_3^{2-}) [30]. A comparison of the catalyst surface element concentrations of 9 % Mn/TiO_2 and 9 % Mn/TiO_2–0.8 % GO in Table 2 shows that introduction of GO not only improves the effective loading capacity of Mn but also enriches the MnO_X species in the catalyst. Introduction of GO also increases the catalytic surface oxygen content, improves the oxygen storage capacity of the catalyst and the redox performance.

3.3 Impacts of H_2O and SO_2

To investigate the effect of H_2O and SO_2 on NO_X conversion of 9 % Mn/TiO_2–0.8 % GO catalyst, the volume fraction of 10 % water vapor and 200 ppm of SO_2 for separate resistance to H_2O and SO_2 experiments were introduced to simulated flue gas for the transient response test. At the same time, 10 % water vapor and 200 ppm SO_2 were fed into the system to carry out water resistance and resistance to sulfur experiments at 180 °C. The effects of H_2O and SO_2 on the catalytic activity of 9 % Mn/TiO_2–0.8 % GO are shown in Fig. 7.

Figure 7 shows that the removal rate of NO_X from the system becomes stable 0.5 h into the reaction. After 2 h, the reaction stabilized when water vapor and SO_2 were

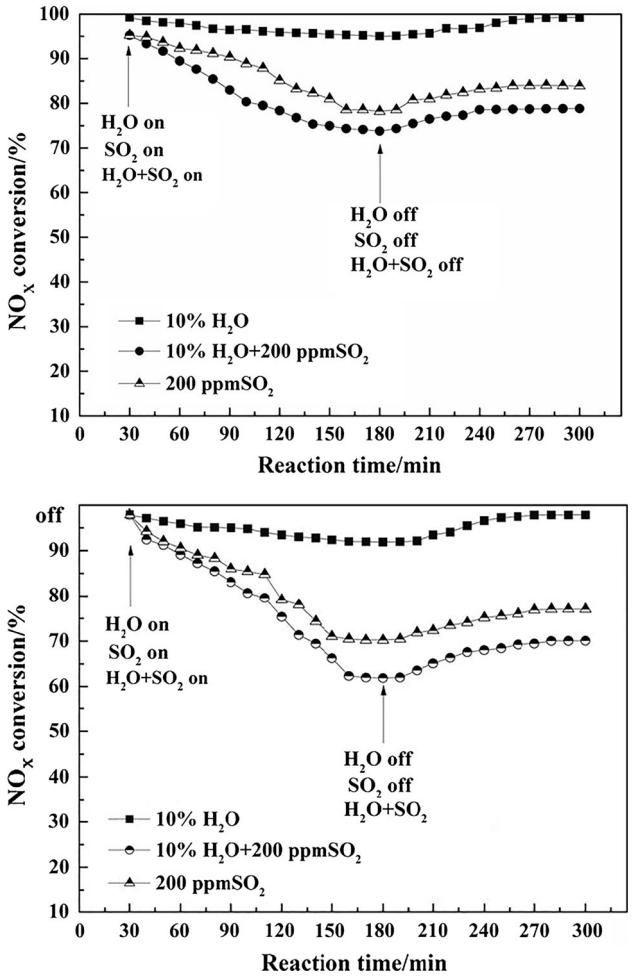

Fig. 7 Effects of H_2O and SO_2 on the catalytic activity of 9 % Mn/TiO_2–0.8 % GO and 9 % Mn/TiO_2

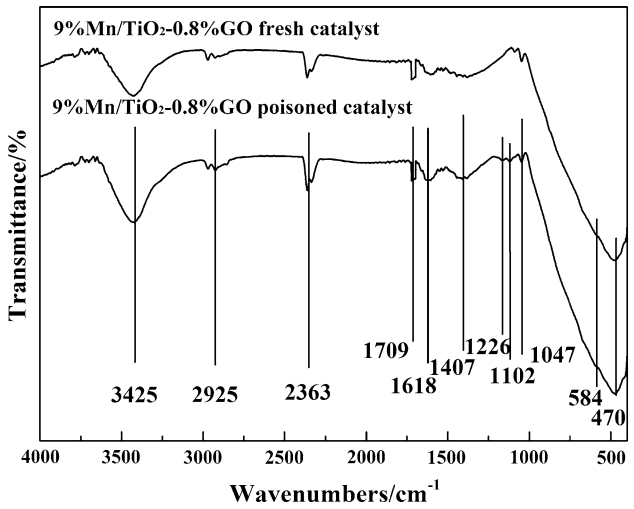

Fig. 8 FT-IR patterns of fresh and poisoned 9 % Mn/TiO_2–0.8 % GO

added to the system to study the influence of poisoning on catalyst activity. Results show that the resistance to H_2O ability of the 9 % Mn/TiO_2–0.8 % GO catalyst is not significantly improved compared with a conventional low temperature SCR catalyst, which is attributed to the GO added to support. The surface of this support has many hydrophilic groups, such as carboxyl, hydroxyl, and epoxy groups. The water vapor can be easily adsorbed onto the catalyst surface and occupy active sites required by NH_3 adsorption, which results in competitive adsorption and a decline in SCR activity. The independent resistance to SO_2 poisoning of the catalyst was significantly improved. The catalytic activity after poisoning stabilized at around 78 %. After SO_2 feeding was removed, the activity of this catalyst was restored to 83 %. The sulfur/water resistance increased to about 73 % and was restored to 79 % when feeding was removed.

The FT-IR spectra of the 9 % Mn/TiO_2–0.8 % GO catalyst before and after poisoning are shown in Fig. 8 for explanation of this phenomenon. Peaks at 2925 and 3425 cm^{-1} are attributed to –OH vibrations, while the peak at 1407 cm^{-1} is attributed to C–OH bond vibrations. The peak at 1618 cm^{-1} is attributed to stretching vibrations of the C–O–C bond, that at 1709 cm^{-1} corresponds to the stretching vibrations of C=O bond, and that at 1226 cm^{-1} is attributed to C–O–C bonds of the epoxy base. At 1102 cm^{-1} of the fresh and poisoned catalyst SO_4^{2-} could be observed, which may result from the large amount of concentrated sulfuric acid during the preparation of GO and is equivalent to the pre-sulfuring of catalyst, thereby inhibiting the sulfation of the active component when SO_2 was fed and substantially increasing resistance to SO_2 ability of the catalyst. The resistance mechanism to SO_2 poisoning of the catalyst needs further research. Taking the results together, a new low temperature SCR catalyst with excellent resistance to sulfur and water was developed in this work. Our work provides a theoretical basis for adding SCR de-nitration devices for sintering flue gas in highly humid, rich in oxygen conditions with a certain amount of sulfur.

4 Conclusion

In summary, TiO_2–GO supports of different Ti/C mass ratios were successfully prepared by using an in situ sol–gel and ultrasonic impregnation methods, which features the largest specific surface area (160 m^2 g^{-1}), showed the best catalytic activity. Through XPS analysis, the high catalytic activity of 9 % Mn/TiO_2–0.8 % GO catalyst was determined to come from introduction of the catalyst, which improves the transfer capability of electrons on the surface. MnO_X of multiple valence was found to exist, and the non-stoichiometric MnO_X/Mn maximize the Redox

capacity of catalyst and significantly enhanced the removal rate of NO_X. Among the catalysts prepared, the 9 % Mn/TiO_2–0.8 % GO catalyst exhibited the highest SCR activity (up to 95 %) at 180 °C, and GHSV of 67,000 h^{-1}. All of the samples showed excellent N_2 selectivity of over 96 %. During investigation of the effects of feeding 10 % water vapor and 200 ppm SO_2 separately into the flue gas at 180 °C on the catalyst activity of 9 % Mn/TiO_2–0.8 % GO, the removal rate of NO_X decreased to 91 % from 95 % before feeding. When feeding of H_2O was stopped for 2 h, the removal rate of NO_X gradually increased to the initial level. When SO_2 was fed separately, the removal rate of NO_X fell to 78 % and returned to 83 % when feeding is stopped. The removal rate of NO_X dropped to 73 % when 10 % H_2O and 200 ppm SO_2 were fed at the same time and was restored to 79 % within 2 h when feeding was stopped. FT-IR analysis showed that introduction of GO induces pre-sulfuration effects on the catalyst itself and inhibits sulfation of the active component. Thus, resistance to H_2O and –SO_2 poisoning in the catalysts is significantly improved. This research provides a theoretical basis for adding SCR de-nitration devices for sintering flue gas in conditions of humidity, rich in oxygen, and with a certain amount of sulfur in the future.

References

1. Fan EY, Wei PB, Sui GR et al (2012) Preparation of Mn-Ce-O_x denitration catalyst and its regeneration performance. Environ Sci Technol 35(9):40
2. Hao J, Wang L, Shen M et al (2007) Air quality impacts of power plant emissions in Beijing. Environ Pollut 147(2):401–408
3. Busca G, Larrubia MA, Arrighi L et al (2005) Catalytic abatement of NO_X: chemical and mechanistic aspects. Catal Today 107–108:139–148
4. Busca G, Lietti L, Ramis G et al (1998) Chemical and mechanistic aspects of the selective catalytic reduction of NO_X by ammonia over oxide catalysts: a review. Appl Catal B Environ 18(1–2):1–36
5. Yao G, Gui K, Wang F (2010) Low-temperature de-NO_X by selective catalytic reduction based on iron-based catalysts. Chem Eng Technol 33(7):1093–1098
6. Park TS, Jeong SK, Hong SH et al (2001) Selective catalytic reduction of nirogen oxides with NH_3 over natural manganese ore at low temperature. Ind Eng Chem Res 40(21):4491
7. Qi G, Yang RT (2003) Low-temperature selective catalytic reduction of NO with NH_3 over iron and manganese oxides supported on titania. Appl Catal B 44(3):217
8. Ettireddy PR, Ettireddy N, Mamedov S et al (2007) Surface characterization studies of TiO_2 supported manganese oxide catalysts for low temperature SCR of NO with NH_3. Appl Catal B 76(1–2):123–134
9. Boningari T, Panagiotis GS (2011) Co-doping a metal (Cr, Fe Co, Ni, Cu, Zn, Ce, and Zr) on Mn/TiO_2 catalyst and its effect on the selective reduction of NO with NH_3 at low-temperatures. Appl Catal B 110(2):195
10. Liu FD, He H, Zhang CB et al (2011) Mechanism of the selective catalytic reduction of NO_x with NH_3 over environmental-friendly iron titanate catalyst. Catal Today 175(1):18
11. Yoshikawa M, Yasutake A, Mochida I (1998) Low-temperature selective catalytic reduction of NO_X by metal oxides supported on active carbon fibers. Appl Catal A Gen 173(2):239–245
12. Tang X, Hao J, Yi H et al (2007) Low-temperature SCR of NO with NH_3 over AC/C supported manganese-based monolithic catalysts. Catal Today 126(3–4):406–411
13. Pradhan BK, Sandle NK (1999) Effect of different oxidizing agent treatments on the surface properties of activated carbons. Carbon 37(8):1323–1332
14. Valdés-Solís T, Marbán G, Fuertes AB (2003) Low-temperature SCR of NO_X with NH_3 over carbon-ceramic supported catalysts. Appl Catal B Environ 46(2):261–271
15. Zhao XY, Ding KQ (2009) Preparation of nano TiO_2/CNTs composite particles and the electrochemical measurement on its ITO film electrode. J Heibei Norm Univ 33(2):214–219
16. Yang D, Rochette J, Sacher E (2005) Functionalization of multiwalled carbon nanotubes by mild aqueous sonication. J Phys Chem B 109(16):7788–7794
17. Hummers WS, Offerman RE (1958) Preparation of graphitic oxide. Carbon 80:1339
18. Stankovich S, Dikin DA, Dommett GHB et al (2006) Graphene-based composite materials. Nature 442:282–286
19. Singoredjo L, Korver R, Kapteijn F et al (1992) Alumina supported manganese oxides for the low-temperature selective catalytic reduction of nitric oxide with ammonia. Appl Catal B 1(4):297–316
20. Chen C, Cai WM, Long MC et al (2010) Synthesis of visible-light responsive graphene oxide/TiO_2 composites with p/n heterojunction. ACS Nano 4(11):6425–6432
21. wang W, Yu J, Xiang Q et al (2012) Enhanced photocatalytic activity of hierarchical macro/mesoporous TiO_2-graphene composites for photodegradation of acetone in air. Appl Catal B Environ 119:109–116
22. Tang X, Hao J, Yi H et al (2007) Low-temperature SCR of NO with NH_3 over AC/C supported manganese-based monolithic catalysts. Catal Today 126(3–4):406–411
23. Lu P, Li C, Zeng G et al (2010) Low temperature selective catalytic reduction of NO by activated carbon fiber loading lanthanum oxide and ceria. Appl Catal B Environ 96(1–2):157–161
24. Planeix JM, Coustel N, Coq B et al (1994) Application of carbon nanotubes as supports in heterogeneous catalysis. J Am Chem Soc 116(17):7935–7936
25. Gao Erping, Wang Wenzhong, Shang Meng et al (2011) Synthesis and enhanced photocatalytic performance of graphene-Bi_2WO_6 composite. Phys Chem Chem Phys 13:2887–2893
26. Akhavan O, Ghaderi E (2009) Photocatalytic reduction of graphene oxide nanosheets on TiO_2 thin film for photoinactivation of bacteria in solar light irradiation. J Phys Chem C 113(47):20214–20220
27. Xiang Q, Jiaguo Y, Jaroniec M (2011) Enhanced photocatalytic H_2-production activity of graphene-modified titania nanosheets. J Nanocale 3:3670–3678
28. Lee JY, Hong SH, Cho SP et al (2006) The study of deNO_X catalyst in low temperature using nano-sized supports. Curr Appl Phys 6(6):996–1001
29. Xining L, Song C, Jia S et al (2015) Low-temperature selective catalytic reduction of NO_X with NH_3 over cerium and manganese oxides supported on TiO_2-graphene. Chem Eng J 260:776–784
30. Ponce S, Peña MA, Fierro JLG (2000) Surface properties and catalytic performance in methane combustion of Sr-substituted lanthanum manganites. Appl Catal B Environ 24(3–4):193–205